ACS OMEGA

Article

http://pubs.acs.org/journal/acsodf

Probing the Catalytic Activity of Sulfate-Derived Pristine and Post-Treated Porous TiO_2(101) Anatase Mesocrystals by the Oxidative Desulfurization of Dibenzothiophenes

Lorena P. Rivoira,[†] Maria L. Martínez,[†] Horacio Falcón,[†] Andrea R. Beltramone,[†] Jose M. Campos-Martin,[‡] Jose L.G. Fierro,[‡] and Pedro Tartaj*[,§]

[†]NANOTEC (Centro de Investigación en Nanociencia y Nanotecnología), Universidad Tecnológica Nacional—Facultad Regional Córdoba, X5016ZAA Córdoba, Argentina

[‡]Energy and Sustainable Chemistry Group (EQS), Instituto de Catálisis y Petroleoquímica, CSIC, Marie Curie 2, Cantoblanco, 28049 Madrid, Spain

[§]Instituto de Ciencia de Materiales de Madrid, CSIC, Cantoblanco, 28049 Madrid, Spain

ABSTRACT: Mesocrystals (basically nanostructures showing alignment of nanocrystals well beyond crystal size) are attracting considerable attention for modeling and optimization of functionalities. However, for surface-driven applications (heterogeneous catalysis), only those mesocrystals with excellent textural properties are expected to fulfill their potential. This is especially true for oxidative desulfuration of dibenzothiophenes (hard to desulfurize organosulfur compounds found in fossil fuels). Here, we probe the catalytic activity of anatases for the oxidative desulfuration of dibenzothiophenes under atmospheric pressure and mild temperatures. Specifically, for this study, we have taken advantage of the high stability of the (101) anatase surface to obtain a variety of uniform colloidal mesocrystals (approximately 50 nm) with adequate orientational order and good textural properties (pores around 3−4 nm and surface areas around 200 m^2/g). Ultimately, this stability has allowed us to compare the catalytic activity of anatases that expose a high number of aligned single crystal-like surfaces while differing in controllable surface characteristics. Thus, we have established that the type of tetrahedral coordination observed in these anatase mesocrystals is not essential for oxidative desulfuration and that both elimination of sulfates and good textural properties significantly improve the catalytic activity. Furthermore, the most active mesocrystals have been used to model the catalytic reaction in three-(oil−solvent−catalyst) and two-phase (solvent−catalyst) systems. Thus, we have been able to observe that the transfer of DBT from the oil to the solvent phase partially limits the oxidative process and to estimate an apparent activation energy for the oxidative desulfuration reaction of approximately 40 kJ/mol in the two-phase system to avoid mass transfer limitations. Our results clearly establish that (101) anatase mesocrystals with excellent textural properties show adequate stability to withstand several post-treatments without losing their initial mesocrystalline character and therefore could serve as models for catalytic processes different from the one studied here.

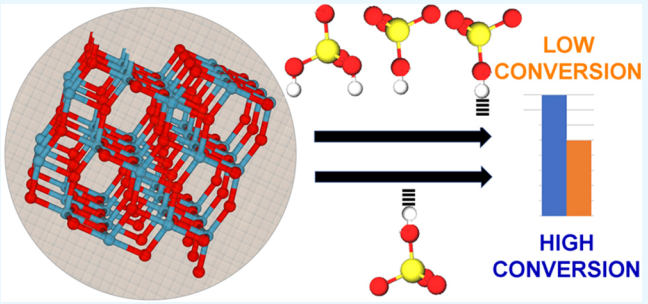

INTRODUCTION

Organosulfur compounds of thiophenic base are toxic pollutants commonly found in fossil fuels (especially in diesel). As they are responsible for air pollution and acid rain (SO_2 formation during combustion), their presence must be minimized.[1−3] However, common desulfurization technologies such as hydrodesulfurization that work relatively well for many sulfur-containing compounds require strongly demanding conditions (high temperature and pressure) when dealing with these sulfur compounds (mainly nonsubstituted and substituted dibenzothiophenes, known as DBTs).[4] Thus, there is special interest to develop less demanding desulfuration processes such as those based on the use of oxidants (oxidative desulfurization, known as ODS). In principle, ODS can be carried out in the liquid phase under very mild conditions (near room temperature and under atmospheric pressure) as thiophenic compounds are among the most oxidizable sulfur compounds.[1−3,5,6] Still ODS faces significant challenges, among them the finding of new solid catalysts that can efficiently catalyze this reaction.[3]

H_2O_2 is often used for sulfoxidation as water is the by-product of the catalytic reaction.[7−9] Previous studies on H/Na titanate nanotubes have shown good oxidation activity in the presence of H_2O_2, though one of the conclusions drawn from that study was that anatase clusters deactivated the catalytic sites.[10] There have been other studies reporting that

Received: March 14, 2017
Accepted: May 4, 2017
Published: May 26, 2017

DOI: 10.1021/acsomega.7b00307
ACS Omega 2017, 2, 2351−2359

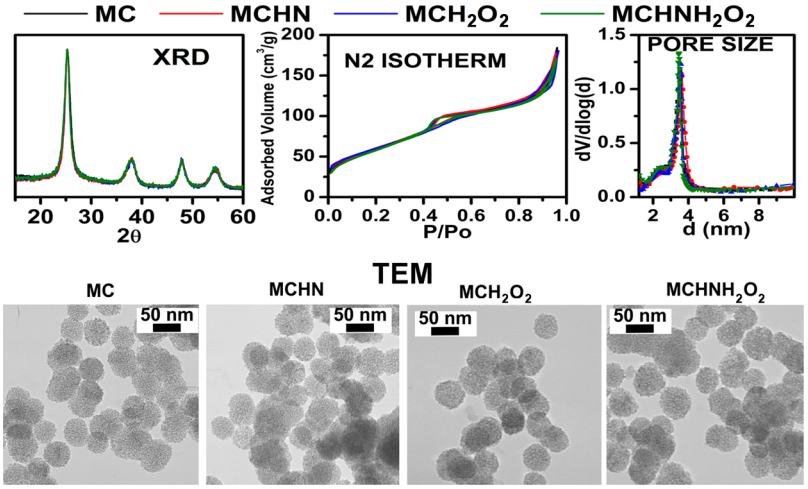

Figure 1. XRD patterns, N_2 isotherms, pore size distribution (BJH model applied to the desorption curve), and TEM for pristine mesocrystals (MC) and those treated with HNO_3 (MCHN), H_2O_2 (MCH_2O_2), or HNO_3 followed by H_2O_2 ($MCHNH_2O_2$). Basically, the structural, microstructural, and textural properties appear similar after the different treatments.

mesoporous anatase doped with phosphotungstic acid (10%) was capable of oxidizing DBTs in combination with H_2O_2.[11,12] However, these studies concluded that the active species for ODS were the phosphotungstic groups. There have been reports that TiO_2 under UV-light irradiation was capable of DBT photo-oxidation,[13,14] but photocatalytic studies are out of the scope of the results presented in this study. However, recent studies on anatases dispersed in mesoporous carbons (obtained after pyrolysis of Ti-based metal−organic frameworks at 600 °C) have shown activity for oxidative desulfuration of DBTs, though in this case the oxidant of choice was *tert*-butyl hydroperoxide.[3] These previous studies, and specially the one of Hicks' group,[3] led us to hypothesize that mesoporous anatases could show adequate activity for oxidative desulfuration of DBTs using H_2O_2 as an oxidant.

Mesocrystals are considered to be the optimal conformations to both enhance and modeling material properties.[15−29] More specifically, titanium oxide mesocrystals have shown improved photocatalytic, optoelectronic, and lithium- and sodium-ion insertion capabilities, and importantly, these unique nanostructures have facilitated a better understanding of the functionality of materials.[23,25,27,29−33] As the activity with solid catalysts mainly originates on surfaces, and different surfaces expose different structural arrangements, the most appropriate methods to study these processes should rely (if possible) on single crystals.[34] Furthermore, single crystals avoid the hurdles of grain boundaries misalignments. However, single crystals lack good textural properties. Mesocrystalline nanostructures are characterized not only by exposing a majority of a single crystal-like surface but also by the alignment of the nanocrystalline building blocks. Indeed, grain boundaries exist, but their effect is minimized by their alignment. Thus, these particular nanostructures should allow closing the gap between nanostructures and single crystals. Obviously, for catalysis, only those mesocrystals with good textural properties are expected to fulfill this goal (there is a need for surface accessibility throughout the volume). This is especially true for the ODS of dibenzothiophenes in the presence of a solid catalyst where high catalytic activities require good textural properties and pore sizes around the mesoscale.[3,7,35−46] Thus, the task is relatively difficult not because of exposing a majority of a unique surface (when dealing with the most stable surface as in anatase this is less difficult) but because of the characteristic alignment of the building nanoblocks must be maintained with pores in between.

The aim of the study here presented is to probe the catalytic activity of high surface area anatases for sulfoxidation of DBTs. More specifically, to probe the catalytic activity of anatases through a variety of porous mesocrystals having similar orientation and textural properties and basically differing only on controllable surface characteristics. As described above, the mesocrystalline character in nanostructures ("the single-crystal behavior") helps to better understand the catalytic processes. Our initial idea is that the use of these well-defined porous nanostructures could help us to better determine limiting factors for sulfoxidation and therefore to identify pathways for further improvement of the catalytic behavior of anatases or other similar materials in this promising desulfuration process.

Recent experimental and theoretical studies have prompted the interest on obtaining anatases, exposing a large fraction of surfaces more reactive than the (101) surface.[47−49] Interestingly, stabilization of these anatase surfaces usually requires dopants or adsorbates, and besides, the resultant textural properties are not as good as the ones required for sulfoxidation of DBTs.[47] However, an important lesson that can be learned from those studies is that if we aim to obtain anatase mesocrystals with good textural properties and relatively good stability to allow some changes on surface characteristics, these porous mesocrystals must expose a large fraction of the energetically stable (101) surface. Some of us have reported that uniform porous anatase mesocrystals with adequate alignment of their constitutive building nanoblocks can be prepared by a combined self-assembly/seeding process [majority of (101) exposed surfaces, uniform colloidal size < 100 nm, Brunauer−Emmett−Teller (BET) areas around 200 m^2/g, and pore size within the mesoscale].[27,30,33] Herein, we use these porous anatase mesocrystals for the oxidative desulfuration of DBTs under atmospheric pressure and mild temperatures. Furthermore, by using simple post-treatments, we are able to modify some surface characteristics while still preserving the mesocrystalline character and textural properties. We understand an additional advantage of these mesocrystals is their colloidal size that allows good dispersibility of the materials when liquid suspensions are involved (oxidative

DOI: 10.1021/acsomega.7b00307
ACS Omega 2017, 2, 2351−2359

desulfuration is carried out in liquid). Detailed characterization of all of these samples has helped us to better understand and to optimize the activity of anatases for sulfoxidation.

RESULTS AND DISCUSSION

Catalysts Characterization. As mentioned in the Experimental Section, the porous anatase mesocrystals used in this study were prepared following a route previously reported by some of us.[33] These mesocrystals were further processed to alter the surface of mesocrystals in a controlled way and later to determine the catalytic response. Specifically, the pristine mesocrystals were treated with HNO_3 and/or H_2O_2 (MCHN, MCH_2O_2, and $MCHNH_2O_2$). Details of the preparation can be found in the Experimental Section. After different post-treatments, preservation of the structural (including phase, size, and mesocrystalline character) and textural characteristics (surface area and pore size) was confirmed by X-ray diffraction (XRD), N_2 isotherms, transmission electron microscopy (TEM), and high-resolution transmission electron microscopy (HR-TEM) (Figures 1 and 2, and Table 1). Basically, all samples are anatase mesocrystals with a majority of (101) exposed surfaces, a similar alignment of the constitutive nanocrystals, a uniform colloidal size (approximately 50 nm), and excellent textural properties for the oxidation of DBT compounds (mesoporous centered at 3.5 nm and surface areas around 200 m^2/g). Preservation of the initial mesocrystalline character of the porous colloidal aggregate was not unexpected once such aggregate is not fragmented during the post-treatments. As described above, the (101) surfaces are the most stable in anatase, and therefore, any rearrangement leading to the formation of other anatase surfaces is unlikely. In fact, one could reasonably argue that the formation of the pristine mesocrystals, in the first place, was only possible because of the presence of majority of the energetically favorable (101) surfaces. Besides, possible crystal misalignments associated with crystal growth are expected to be limited by the fact that anatase crystal sizes remained similar after post-treatments.

X-ray photoelectron spectra (XPS), thermogravimetric (TG) curves, infrared (IR), and ultraviolet−visible (UV−vis) studies were carried out to estimate the surface characteristics of all mesocrystals (including the pristine mesocrystals not previously characterized using these techniques). For example, $TiOSO_4$ was used as a precursor for the synthesis of pristine mesocrystals. Sulfate groups remaining on the surface are known to alter the catalytic activity of anatases.[34] Figure 3 shows the XPS of Ti 2p and S 2p core levels for all samples. For Ti 2p levels, the doublet arises from spin-orbit splitting Ti $2p_{3/2}$ and Ti $2p_{1/2}$.[50] The analysis of the Ti $2p_{3/2}$ levels (more intense

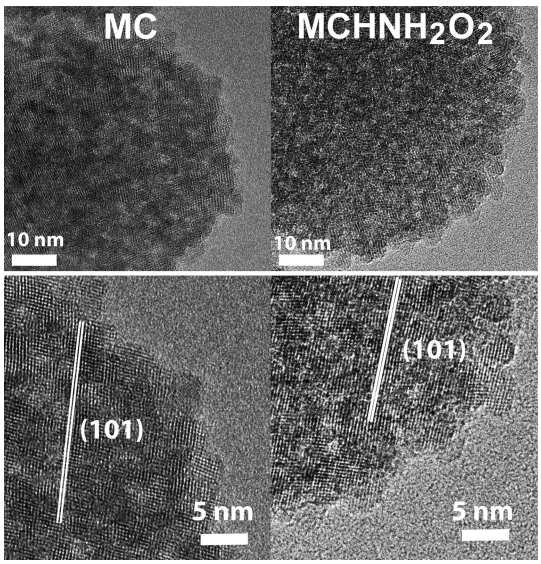

Figure 2. HR-TEM pictures at different magnifications of the pristine mesocrystals (MC) and the most severely post-treated mesocrystals ($MCHNH_2O_2$, treatment HNO_3 followed by H_2O_2). The pictures show that $MCHNH_2O_2$ preserves the mesocrystalline character similar to that of the pristine mesocrystals. In both samples, anatase nanocrystals within the colloidal aggregate appear aligned in a preferential direction over extensive areas with majority of (101) exposed surfaces.

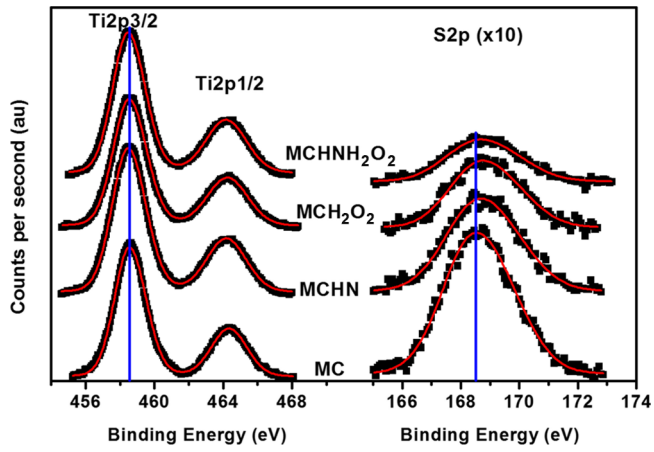

Figure 3. XPS spectra corresponding to the Ti 2p and S 2p core levels for all samples. The signal for S 2p was increased approximately 10 times with respect to Ti 2p for a better visualization. Exact quantification of the Ti/S molar ratio derived from the spectra is given in Table 1.

Table 1. Textural Characteristics, Core Level XPS Binding Energies (eV), S/Ti Atomic Ratios Obtained from Both XPS and TG Analyses, and TG Losses (150−450 °C) for Pristine and Post-Treated Mesocrystalline Anatases[a]

	textural properties			XPS				TG	
sample	BET (m^2/g)	pore size[b] (nm)	pore volume (cm^3/g)	Ti $2p_{3/2}$	S 2p	O 1s	S/Ti	S/Ti	loss 150−450 °C (%)
MC	210	3.5	0.30	458.6	168.5	529.6/531.5	0.16	0.10	2.0
MCHN	220	3.6	0.29	458.6	168.7	529.7/531.5	0.11	0.06	3.7
MCH_2O_2	220	3.6	0.29	458.6	168.8	529.8/531.5	0.07	0.035	4.3
$MCHNH_2O_2$	220	3.5	0.30	458.6	168.8	529.9/531.5	0.05	0.025	3.8

[a]As mentioned in the article, MC are the pristine mesocrystals, and MCHN, MCH_2O_2, and $MCHNH_2O_2$ are mesocrystals treated with HNO_3, H_2O_2, and HNO_3 followed by H_2O_2, respectively. [b]Pore size distribution maximum from BJH model applied to the desorption curve.

DOI: 10.1021/acsomega.7b00307
ACS Omega 2017, 2, 2351−2359

signal) shows the binding energy values of Ti $2p_{3/2}$ in all samples (Table 1) corresponding to Ti^{4+} (458.6 eV).[51,52] The similarity in Ti $2p_{3/2}$ binding energy values for all samples and the fact that no additional signals were detected at lower binding energies (Ti^{3+} is characterized by a shoulder, shifted approximately 2 eV to lower energy) suggest that the post-treatment did not alter the Ti framework. Perhaps, the most relevant result derived from the XPS study comes from the analysis of the S 2p levels. Figure 3 and Table 1 shows the binding energy values (approximately 168.5−168.7 eV) that can be assigned to sulfate moieties.[53] An analysis of their respective areas indicates a significant decrease in the sulfate level with post-treatments (Table 1). A slight but systematic shift in the position of the maxima was observed after different treatments. However, the poor signal quality (especially for the H_2O_2-treated mesocrystals where sulfate content is low) along with the slight shift precluded a meaningful analysis on the nature of sulfate moieties. Furthermore, the conditions in which XPS were recorded (ultrahigh vacuum) intrinsically limit the capability of this technique to unequivocally determine the nature of sulfate species under operating conditions. As we better describe below, this analysis was carried out using IR spectroscopy. Finally, we must mention that the analysis of the O 1s core levels (Table 1) showed the typical titania signals assigned to lattice oxygens (∼530 eV) and commonly to OHs (531.5 eV).[52,54,55] Table 1 summarizes the XPS binding energy values for the different species.

OH studies using XPS are certainly limited by the fact that the spectra were registered under ultrahigh vacuum conditions (10^{-9} Torr). Therefore, we carried out TG studies to basically estimate whether the removal of sulfate generated new chemisorbed OH species and to simultaneously extract some information on sulfate losses. The results of this characterization are shown in Figure 4 and Table 1. We have also included the TG analysis of titania P25 from Degussa (the standard for comparison, 50 m^2/g). We must keep in mind that P25 is free of sulfates (obtained from gas-phase flame synthesis using $TiCl_4$ as a precursor). First, Figure 4 shows a significant loss above 500 °C that must be mainly associated with sulfates.[34,56] Supporting this interpretation, TG losses above this temperature follow the same trend as that estimated by XPS for the content of sulfates (MC > MCHN > MCH_2O_2 > $MCHNH_2O_2$). Table 1 shows the estimation of the S/Ti molar ratio in samples by assuming that these losses mainly come from sulfates. As expected, we observe an enrichment of sulfates on the surface (S/Ti molar ratio from XPS higher than TG). Furthermore, the specifics of sulfate losses are certainly ambiguous. Indeed, the sulfate losses occur earlier for pristine mesocrystals, but the end point is detected at lower temperatures for H_2O_2-treated samples (∼470−820 °C = 350 °C for MC vs ∼630−760 °C = 130 °C for $MCHNH_2O_2$). The slower rate for the pristine mesocrystals could be understood in terms of a much broader distribution on sulfate bonding strengths. Basically, sulfates on H_2O_2-treated mesocrystal surfaces are lower in content and are more homogenous. Regarding the content of chemisorbed water on samples (say OHs), a TG temperature region between 120 and 500 °C is often used to estimate a significant portion of these species.[57] However, the lower limit (exclusion of physisorbed water) depends on experimental conditions, whereas in our case the upper limit slightly overlaps with the sulfate elimination. Therefore, in Table 1, we show the losses corresponding to the interval 150−450 °C. The pristine mesocrystals have the highest content of sulfates and the lowest content of chemisorbed OH species. However, all post-treated mesocrystals have similar content of chemisorbed OH species despite the different sulfate content. These findings indicate no straightforward correlation between the sulfate losses and OH generation. Importantly, these results also seem to suggest that the surface of the mesocrystals reaches saturation on chemisorbed OHs.

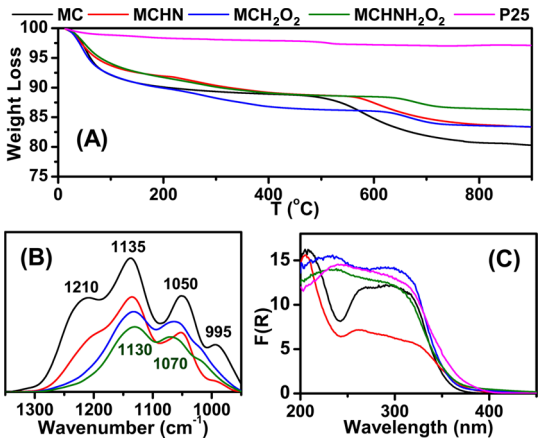

Figure 4. (A) TG curves, (B) IR spectra in the sulfate region after background subtraction, and (C) diffuse reflectance UV−vis spectra ($F(R) = (1 - R)^2/2R$) for all mesocrystals. As described in the main text, MC corresponds to the pristine anatase mesocrystals, and MCHN, MCH_2O_2, and $MCHNH_2O_2$ corresponds to the post-treated mesocrystals with HNO_3, H_2O_2, and HNO_3 followed by H_2O_2, respectively. Titania P25 from Degussa is also included in the TG and diffuse reflectance characterization.

As reported above, TG results on sulfate losses are certainly ambiguous and could be understood in terms of a much broader distribution on sulfate bonding strengths of pristine when compared with post-treated mesocrystals. Furthermore, XPS analysis is limited by the fact that the spectra were registered under ultrahigh vacuum conditions (10^{-9} Torr) and the low content of sulfates (especially for H_2O_2-treated samples). Thus, additional information on the nature of the sulfate groups anchored to the surfaces was obtained from the analysis of the IR spectra in the 1350−950 cm^{-1} region, where typically sulfate and bisulfate ligands are detected.[58−62] Specifically, in the pristine mesocrystals, absorption bands at 1210, 1135, 1050, and 995 cm^{-1} are clearly detected (Figure 4). For post-treated mesocrystals, the band at 1210 cm^{-1} decreases in intensity to finally disappear in the H_2O_2-treated mesocrystals. The bands at 1135, 1050, and 995 cm^{-1} also appear less intense or almost disappear, and importantly, the separation between these bands (splitting) is less marked as the content of sulfate diminishes in samples. Unambiguous assignation of these bands is rather difficult as their position is within the range expected for monodentate/bidentate sulfates, H-bonded sulfates, or bisulfate ligands. However, the attachment of sulfates to the surfaces is understood in terms of the loss in symmetry from a regular T_d symmetry (free sulfates), to a distorted T_d symmetry (outer-sphere complexes), and to C_{3v} and C_{2v} symmetries (inner-sphere complexes), with the subsequent loss in degeneration (new bands appear).[58] Thus, the combination of IR and TG results suggest that pristine mesocrystals contain a variety of strongly and weakly interacting inner- and outer-sphere sulfate surface complexes,

DOI: 10.1021/acsomega.7b00307
ACS Omega 2017, 2, 2351−2359

whereas weakly outer-sphere sulfate complexes are likely predominant in post-treated samples (specially H_2O_2-treated).

The existence of isolated Ti(IV) sites tetrahedrally coordinated by Si−O and OHs in titanias highly dispersed in amorphous/mesoporous silica or zeolitic silicates is well-established.[35,63−65] In fact, several studies have shown that oxidative desulfuration reactions are catalyzed by these species.[7,35,38,43] Interestingly, even though the (101) surface is characterized by the presence of 5- and 6-fold titanium coordination,[48,66] the existence of a 4-fold coordination has also been reported in high surface area (101) anatases and often interpreted on the basis of the existence at the surfaces of amorphous domains or simply defective disordered clusters.[67−69] Thus, to draw some conclusions on the catalytic activity of pristine and post-treated mesocrystals toward the oxidation of DBTs, there is a need to determine the coordination environment of Ti(IV) ions. UV−vis diffuse reflectance spectroscopy represents a relatively simple and sensitive technique to determine Ti(IV) coordination on solid samples, as ligand-to-metal charge transfer processes are detected between 200 and 400 nm.[63,64,70] Specifically, bands below approximately 230 nm have been associated with the tetrahedral coordination. Above 230 nm, bands have been typically associated with either 5- or 6-fold coordinations.[64,70−72] At longer wavelengths, the spectra display the typical broad features of bulk anatase and/or the standard for catalytic studies (titania P25 from Degussa). Thus, UV−vis spectra were recorded for all mesocrystalline samples with titania P25 included for comparison (Figure 4). At 205−210 nm, both pristine (MC) and HNO_3-treated (MCHN) mesocrystals show an intense absorption band associated with the tetrahedral coordination.[7,63−65] Both MC and MCHN samples contain a significant amount of sulfate groups that could partially contribute to the 4-fold coordination (Ti−O−S bonds). The presence of these bonds would support the above-mentioned presence of strongly interacting inner-sphere sulfate complexes in non-H_2O_2-treated samples. However, the band is more intense for MCHN despite containing lower content of sulfates. This result seems to suggest that acidic conditions favor the stabilization of tetrahedral environments. Following this argument, the stabilization of the tetrahedral coordination in the pristine mesocrystals could be partially explained by the fact that hydrolysis/condensation of $TiOSO_4$ precursors is carried out in strongly acid media ($TiOSO_4$ is dissolved in concentrated H_2SO_4). The spectra for MCH_2O_2 and $MCHNH_2O_2$ (H_2O_2 treatment was the latest for both samples) resemble that of P25. The bands associated with the tetrahedral coordination disappear, supporting the argument that this coordination is stabilized under strong acidic conditions. The distinguishing broad feature that appears at approximately 230 nm could be assigned to either polymeric 5-fold titania species or octahedral coordination associated with the insertion of water molecules as extraligands.[64,70−72] Peroxo or superoxide groups seem to be excluded as they usually lead to absorption bands at approximately 400−450 nm.[73] These groups are characterized by their poor stability even at room temperature,[74] and their absence must be associated with the washing and drying protocols (60 °C under vacuum) carried out after the H_2O_2 treatment.

Catalytic Performance. To evaluate the catalytic activity of the samples, a three-phase liquid−liquid−solid [L (oil)−L (solvent)−S (catalyst)] system was simulated, using *iso*-octane as the oil phase and acetonitrile as the solvent (polar) phase. The accepted mechanism for oxidative desulfuration of DBTs occurs by simultaneous extraction/oxidation of DBT in the solvent solution in the presence of the catalyst and the oxidant. Figure 5A shows the catalytic activity of pristine (MC) and post-treated mesocrystals (MCHN, MCH_2O_2, and $MCHNH_2O_2$). The catalytic activity of titania P25 (Degussa, 50 m^2/g) is also included for comparison (free of sulfates). Figure 5A clearly shows that there is an inverse correlation between the sulfate content and the catalytic activity for the mesocrystalline samples. As described above, the IR and TG analyses suggested that in post-treated mesocrystals (especially H_2O_2-treated) not only the content of sulfates was lower but also the interaction with the surface seemed to be lower. Thus, the results shown in Figure 5A clearly indicate that for the oxidative desulfuration reaction, sulfate groups inhibit the catalytic activity. Furthermore, we also show that the sulfoxidation of DBTs does not require Ti(IV) in tetrahedral coordination, unlike what is observed in titanias isolated on high surface area silica or silicalite. $MCHNH_2O_2$, the most active mesocrystalline sample, also has a lower sulfate content, and therefore, its activity is comparable with that of P25 (no sulfates). After 10 min (Figure 5A), the catalytic activity of $MCHNH_2O_2$ doubles that of P25, even though $MCHNH_2O_2$ still contains some residual sulfates that as reported above inhibit the catalytic activity. These results clearly reflect the better textural properties of the mesocrystals when compared with P25. Basically, despite $MCHNH_2O_2$ still contains some sulfates, the higher surface area when compared with P25 (200 vs 50 m^2/g) assures more active sites available for sulfoxidation.

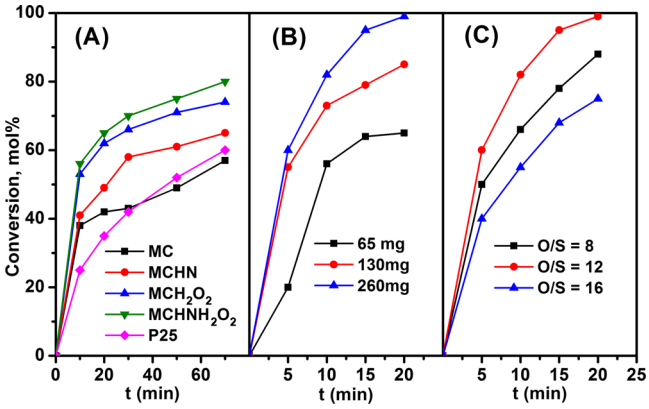

Figure 5. (A) Conversion efficiency of pristine and post-treated mesocrystals for oxidative desulfuration of DBTs. The results for P25 from Degussa are also shown. (B) Conversion efficiency as a function of the amount of catalyst $MCHNH_2O_2$ and (C) conversion efficiency as a function of the H_2O_2 content (expressed as O/S ratio) using $MCHNH_2O_2$ as the catalyst. The reaction conditions were as follows: for (A) 60 °C, 0.065 g of catalyst and oxidant/S (O/S) molar ratio of 12; for (B) 60 °C, O/S molar ratio of 12 with the amount of $MCHNH_2O_2$ changing; for (C) 60 °C, 0.260 g of catalyst with O/S molar ratio changing. In all cases, we use 350 ppm of S (in DBT) dissolved in 65 mL of *iso*-octane and 12.5 mL of acetonitrile.

Figure 5A shows that the activity of the catalyst $MCHNH_2O_2$ reaches good conversion (80%) after 70 min of reaction time but at a relatively slow rate. To improve the conversion rate for this catalyst, we have modified several parameters. Figure 5B shows the catalytic activity after increasing the amount of $MCHNH_2O_2$ catalyst (from 0.065 to 0.260 g). Increasing the amount of the catalysts leads to an increase in the conversion

DOI: 10.1021/acsomega.7b00307
ACS Omega 2017, 2, 2351−2359

rate. Full conversion was achieved only after 20 min using 0.260 g of catalyst under the same conditions. Figure 5C shows the catalytic performance at different H_2O_2 amounts (expressed as O/S molar ratios). Increasing the O/S molar ratio leads to an increase in conversion, reaching a maximum around a molar ratio of 12. A similar trend has been observed for H/Na titanate nanotubes and for the photocatalytic-assisted oxidation of DBTs by anatase.[10,13] The decrease in conversion at high H_2O_2 concentrations could be due to unproductive H_2O_2 decomposition and/or possible poisoning of active sites.[10,13] We must mention that O/S values can be considered high when compared with systems using oxidants such as cyclohexanone peroxidase[75,76] but are in the range expected using H_2O_2 as an oxidant.[9,11,77−80] As mentioned earlier, H_2O_2 assures water as the by-product of the catalytic reaction, and the cost is low when compared with other oxidants.

Transfer of organosulfur compounds from the oil to the solvent phase usually represents a limiting factor on sulfoxidation reactions. Thus, the effect of mass transfer limitations has been also studied using the most active catalyst ($MCHNH_2O_2$) in the three-phase system configuration described above and a two-phase L (solvent)−S (catalyst) system configuration (Figure 6A). Higher conversions were

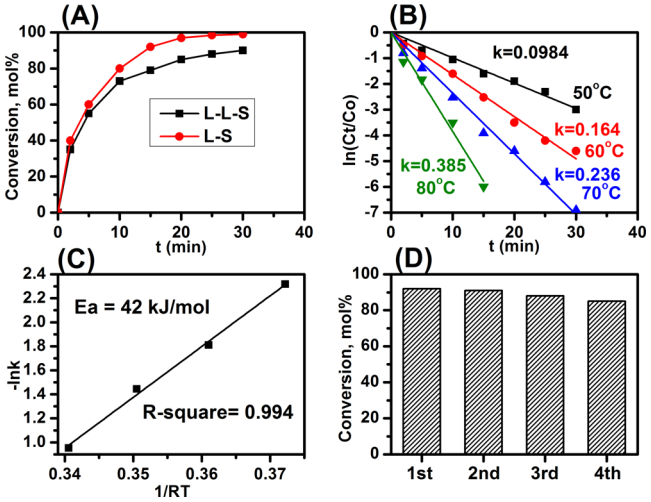

Figure 6. (A) Conversion efficiency for sample $MCHNH_2O_2$ in a three-phase (L−L−S; *iso*-octane−acetonitrile−catalyst) and a two-phase system (L−S; acetonitrile−catalyst). (B) Specific rate constant (k) at different temperatures derived from a pseudo-first-order equation ($\ln(C_t/C_0) = -kt$) with C_0 and C_t being the concentration of DBT at t = 0 and t min, respectively. (C) Arrhenius plot ($k = A\exp(E_a/RT)$) used to determine the apparent activation energy (E_a) for the oxidation reaction with A being the pre-exponential factor, and R and T having the usual meaning. (D) Cyclability studies. The conditions for registering curve in (A) were T = 60 °C, O/S molar ratio = 12, and 0.130 g of catalyst. For (B) and (C), O/S = 12 and 0.130 g of catalyst in an L−S system. For (D), T = 60 °C, O/S = 12, 0.130 g of catalyst, and 15 min of reaction time in an L−S system. In (D), previous to each test, the sample was washed several times with a water−methanol solution.

obtained in the L−S system, demonstrating the existence of mass transfer limitations. This result means that the liquid−liquid extraction step does not occur fast enough and that the transfer of DBT from the oil phase to the solvent phase limits the global rate of the ODS process. The difference was small at the beginning of the reaction and increased to ∼15% after 10 min of reaction time, suggesting that mass transfer limitations become more important at longer times.

Finally, the most active catalyst ($MCHNH_2O_2$) was used to obtain kinetic parameters. As a three-phase L−L−S system suffers from mass transfer limitations, a two-phase L−S system was used to obtain those kinetic parameters (Figure 6B). A pseudo-first-order rate model was found to be reasonable fit for the experimental data obtained at four studied temperatures (50, 60, 70, and 80 °C). The specific rate constant values (k) derived from the pseudo-first-order rate equation were used to obtain an apparent activation energy (E_a) using the Arrhenius equation (Figure 6C). The value (approximately 40 kJ/mol) is within the range obtained for H/Na titanate nanotubes (45 kJ/mol), polyoxometalates (55 kJ/mol), Ti-based metal−organic frameworks (75 kJ/mol), and phosphotungstic-doped TiO_2 matrixes (55 kJ/mol).[10,46,81,82] Preliminary studies on the cyclability of the catalyst were carried out to determine its reusability (Figure 6D). The conversion efficiency diminished only less than 10% after 4th cycle.

CONCLUSIONS

In summary, we have established that (101) anatase mesocrystals of a monodisperse colloidal size and excellent textural properties show adequate stability to withstand several post-treatments without losing their mesocrystalline character. This stability has allowed us to determine some limiting factors for efficient oxidative desulfuration of DBTs. Thus, we have shown that sulfate groups inhibit the catalytic activity. We have also shown that the type of tetrahedral coordination observed in these anatase mesocrystals is not essential for the oxidation of DBTs, unlike to what is observed in titanias highly diluted in amorphous/mesoporous silica or zeolitic silicates. Catalytic studies using optimized mesocrystals have allowed us to conclude that the transfer of DBT from the oil to the solvent phase partially limits the sulfoxidation process and to estimate an apparent activation energy for the sulfoxidation reaction of approximately 40 kJ/mol. Finally, our results suggest that (101) mesocrystals with good textural properties could serve as excellent models for mechanistic studies in other catalytic processes different from the one studied here.

EXPERIMENTAL SECTION

Mesocrystals Synthesis, Postprocessing Protocols Using HNO_3 and/or H_2O_2, and Nomenclature. The porous anatase mesocrystals used in this study were prepared following a route previously reported by some of us.[33] The method consists of seeded-assisted hydrolysis/condensation of $TiOSO_4$ dissolved in nanomicelles undergoing a self-assembly process driven by temperature. Details of the protocol can be found in ref 33.

Postsynthesis treatment of mesocrystals consisted of their processing with HNO_3 and/or H_2O_2. The HNO_3 treatment consisted of dispersing 250 mg of mesocrystals in 20 mL of a 0.1 M HNO_3 aqueous solution followed by 24 h stirring, centrifugation, washing with water several times, and finally drying at 60 °C in a vacuum oven. The H_2O_2 treatment was similar to the HNO_3 treatment, though in this case a H_2O_2 (50 wt %) solution was used, and the stirring was limited to 10 min. Some mesocrystals were treated with both HNO_3 and H_2O_2 (HNO_3 followed by H_2O_2). The samples were named MC (pristine mesocrystals derived from the synthesis), MCHN (post-treatment with HNO_3), MCH_2O_2 (post-treatment with

DOI: 10.1021/acsomega.7b00307
ACS Omega 2017, 2, 2351−2359

H_2O_2), and $MCHNH_2O_2$ (post-treatment with HNO_3 followed by H_2O_2).

Characterization Methods. Phase identification was performed by X-ray diffraction analysis using a Bruker D8 Advance instrument (Cu Kα radiation, 40 kV, 30 mA). The crystal domain size was determined from the X-ray profiles using the Scherrer equation. The morphology, particle size, and crystallinity of the mesocrystals were examined using TEM (2000 FX2, JEOL) and HR-TEM (300, JEOL). Nitrogen adsorption−desorption isotherms were performed at −196 °C in a Micromeritics ASAP 2010 volumetric adsorption system. The BET surface area was deduced from the analysis of the isotherm at low pressures (0.05 to 0.20), whereas pore size distributions were estimated using the Barrett−Joyner−Halenda (BJH) model applied to the desorption curve. TG curves were recorded in a Seiko EXSTAR 6300 instrument under air atmosphere (100 mL/min) and with a ramp of 5 °C/min. Infrared spectra were recorded in a Bruker IFS 66V-S instrument by diluting the samples in a KBr pellet. UV−vis diffuse reflectance spectra were recorded on a Varian Cary 5000 spectrophotometer equipped with an integrating sphere. A $BaSO_4$ disk was used as a reference. All spectra were recorded under ambient conditions. X-ray photoelectron spectra (XPS) registered under ultrahigh vacuum conditions (10^{-9} Torr) were recorded on a MicrotechMultilb 3000 spectrometer. The spectrometer is equipped with a hemispherical electron analyzer and an Mg Kα ($h\nu$ = 1253.6 eV) photon source. An estimated error of ±0.1 eV can be assumed for all measurements. The peak intensity was calculated from the respective peak areas after background subtraction and spectrum fitting by a combination of Gaussian/Lorentzian functions.

Catalytic Experiments. The catalytic sulfoxidation of DBTs with hydrogen peroxide was carried out batchwise in a mechanically stirred 250 mL thermostated glass reactor equipped with a thermometer, a reflux condenser, and a septum for withdrawing samples. In a typical experiment, 65 mL of 350 ppm of sulfur as DBT in *iso*-octane (Aldrich, 99 wt %) was heated to 60 °C. Then, 12.5 mL of acetonitrile was added to the nonpolar phase, and the catalyst (0.065 g) was loaded into the reactor at atmospheric pressure. Finally, a solution of hydrogen peroxide (50 wt %) was introduced into the reactor. Aliquots were taken from the reactor at different reaction times. Importantly, the total amount withdrawn from the reactor was less than 10% to avoid interference in the reaction results because of the changes in the total mass inside of the reactor. The nonpolar phase was recovered by decantation and analyzed by a GC-PFPD (HP5890) instrument equipped with a capillary column (HP-WAX, 25 m, 0.53 mm, and 1.0 mm film thickness). The presence of oxidized products in polar acetonitrile was confirmed by GC−mass spectrometry (HP5890).

The conversion of DBT was calculated by checking the remaining sulfur in both phase systems: L−S and L−L−S. The conversion of DBT was calculated according to the following equation $X_{DBT} = ((C_0 - C_t)/C_0) \times 100\%$, with C_0 and C_t being the concentration of DBT at t = 0 and t min, respectively. Aliquots were taken from the oil phase at different reaction times after decantation and analyzed by a GC-PFPD (HP5890) instrument equipped with a capillary column (HP-WAX, 25 m, 0.53 mm, and 1.0 mm film thickness) using *n*-decane as an external standard. Importantly, the total amount withdrawn from the reactor was less than 10% to avoid interference in the reaction results because of the changes in the total mass inside of the reactor. The presence of oxidized products in polar acetonitrile was confirmed by GC−mass spectrometry (HP5890) and compared with the available standard compounds where available.

To determine the specific rate constant (k) at different temperatures, we used a pseudo-first-order equation ($\ln(C_t/C_0) = -kt$), with C_0 and C_t being the concentration of DBT at t = 0 and t min, respectively. The Arrhenius plot ($k = A \exp(E_a/RT)$) was used to determine the apparent activation energy (E_a) for the oxidation reaction, with A being the pre-exponential factor and R and T being the gas constant and temperature in kelvin, respectively.

AUTHOR INFORMATION

Corresponding Author

*E-mail: ptartaj@icmm.csic.es (P.T.).

ORCID

Pedro Tartaj: 0000-0001-7323-1545

Notes

The authors declare no competing financial interest.

ACKNOWLEDGMENTS

M.L.M., H.F., and A.R.B. are researchers from CONICET. The authors thank CONICET Argentina, PIP CONICET 11220120100218CO, 2014−2017. P.T. acknowledges the financial support from MINECO Spain under contract MAT2014-54994-R.

REFERENCES

(1) Campos-Martin, J. M.; Capel-Sanchez, M. C.; Perez-Presas, P.; Fierro, J. L. G. Oxidative Processes of Desulfurization of Liquid Fuels. *J. Chem. Technol. Biotechnol.* **2010**, *85*, 879−890.

(2) Anisimov, A. V.; Tarakanova, A. V. Oxidative Desulfurization of Hydrocarbon Raw Materials. *Russ. J. Gen. Chem.* **2009**, *79*, 1264−1273.

(3) McNamara, N. D.; Kim, J.; Hicks, J. C. Controlling the Pyrolysis Conditions of Microporous/Mesoporous MIL-125 To Synthesize Porous, Carbon-Supported Ti Catalysts with Targeted Ti Phases for the Oxidation of Dibenzothiophene. *Energy Fuels* **2016**, *30*, 594−602.

(4) Babich, I. V.; Moulijn, J. A. Science and Technology of Novel Processes for Deep Desulfurization of Oil Refinery Streams: A Review. *Fuel* **2003**, *82*, 607−631.

(5) Qiu, L.; Cheng, Y.; Yang, C.; Zeng, G.; Long, Z.; Wei, S.; Zhao, K.; Luo, L. Oxidative Desulfurization of Dibenzothiophene Using a Catalyst of Molybdenum Supported on Modified Medicinal Stone. *RSC Adv.* **2016**, *6*, 17036−17045.

(6) Long, Z.; Yang, C.; Zeng, G.; Peng, L.; Dai, C.; He, H. Catalytic Oxidative Desulfurization of Dibenzothiophene Using Catalyst of Tungsten Supported on Resin D152. *Fuel* **2014**, *130*, 19−24.

(7) Capel-Sanchez, M. C.; Campos-Martin, J. M.; Fierro, J. L. G. Removal of Refractory Organosulfur Compounds via Oxidation with Hydrogen Peroxide on Amorphous Ti/SiO_2 Catalysts. *Energy Environ. Sci.* **2010**, *3*, 328−333.

(8) Campos-Martin, J. M.; Capel-Sanchez, M. C.; Fierro, J. L. G. Highly Efficient Deep Desulfurization of Fuels by Chemical Oxidation. *Green Chem.* **2004**, *6*, 557.

(9) Capel-Sanchez, M. C.; Perez-Presas, P.; Campos-Martin, J. M.; Fierro, J. L. G. Highly Efficient Deep Desulfurization of Fuels by Chemical Oxidation. *Catal. Today* **2010**, *157*, 390−396.

(10) Lorençon, E.; Alves, D. C. B.; Krambrock, K.; Ávila, E. S.; Resende, R. R.; Ferlauto, A. S.; Lago, R. M. Oxidative Desulfurization of Dibenzothiophene over Titanate Nanotubes. *Fuel* **2014**, *132*, 53−61.

(11) Huang, D.; Wang, Y. J.; Cui, Y. C.; Luo, G. S. Direct Synthesis of Mesoporous TiO_2 and Its Catalytic Performance in DBT Oxidative Desulfurization. *Microporous Mesoporous Mater.* **2008**, *116*, 378−385.

DOI: 10.1021/acsomega.7b00307
ACS Omega 2017, 2, 2351−2359

(12) Huang, D.; Wang, Y. J.; Yang, L. M.; Luo, G. S. Chemical Oxidation of Dibenzothiophene with a Directly Combined Amphiphilic Catalyst for Deep Desulfurization. *Ind. Eng. Chem. Res.* **2006**, *45*, 1880−1885.
(13) Matsuzawa, S.; Tanaka, J.; Sato, S.; Ibusuki, T. Photocatalytic Oxidation of Dibenzothiophenes in Acetonitrile Using TiO_2: Effect of Hydrogen Peroxide and Ultrasound Irradiation. *J. Photochem. Photobiol., A* **2002**, *149*, 183−189.
(14) Robertson, J.; Bandosz, T. J. Photooxidation of Dibenzothiophene on TiO_2/hectorite Thin Films Layered Catalyst. *J. Colloid Interface Sci.* **2006**, *299*, 125−135.
(15) Li, Z.; Dong, C.-K.; Yang, J.; Qiao, S.-Z.; Du, X.-W. Laser Synthesis of Clean Mesocrystal of Cupric Oxide for Efficient Gas Sensing. *J. Mater. Chem. A* **2016**, *4*, 2699−2704.
(16) Cölfen, H.; Antonietti, M. Mesocrystals: Inorganic Superstructures Made by Highly Parallel Crystallization and Controlled Alignment. *Angew. Chem., Int. Ed.* **2005**, *44*, 5576−5591.
(17) De Yoreo, J. J.; Gilbert, P. U. P. A.; Sommerdijk, N. A. J. M.; Penn, R. L.; Whitelam, S.; Joester, D.; Zhang, H.; Rimer, J. D.; Navrotsky, A.; Banfield, J. F.; et al. Crystallization by Particle Attachment in Synthetic, Biogenic, and Geologic Environments. *Science* **2015**, *349*, aaa6760.
(18) Zhou, L.; O'Brien, P. Mesocrystals—Properties and Applications. *J. Phys. Chem. Lett.* **2012**, *3*, 620−628.
(19) Tachikawa, T.; Majima, T. Metal Oxide Mesocrystals with Tailored Structures and Properties for Energy Conversion and Storage Applications. *NPG Asia Mater.* **2014**, *6*, No. e100.
(20) Ma, M.-G.; Cölfen, H. Mesocrystals—Applications and Potential. *Curr. Opin. Colloid Interface Sci.* **2014**, *19*, 56−65.
(21) Liu, Y.; Zhang, Y.; Wang, J. Mesocrystals as a Class of Multifunctional Materials. *CrystEngComm* **2014**, *16*, 5948−5967.
(22) Tartaj, P.; Amarilla, J. M. Porous Inorganic Nanostructures with Colloidal Dimensions: Synthesis and Applications in Electrochemical Energy Devices. *Chem. Commun.* **2014**, *50*, 2077−2088.
(23) Crossland, E. J. W.; Noel, N.; Sivaram, V.; Leijtens, T.; Alexander-Webber, J. A.; Snaith, H. J. Mesoporous TiO_2 Single Crystals Delivering Enhanced Mobility and Optoelectronic Device Performance. *Nature* **2013**, *495*, 215−219.
(24) Popovic, J.; Demir-Cakan, R.; Tornow, J.; Morcrette, M.; Su, D. S.; Schlögl, R.; Antonietti, M.; Titirici, M.-M. $LiFePO_4$ Mesocrystals for Lithium-Ion Batteries. *Small* **2011**, *7*, 1127−1135.
(25) Ye, J.; Liu, W.; Cai, J.; Chen, S.; Zhao, X.; Zhou, H.; Qi, L. Nanoporous Anatase TiO_2 Mesocrystals: Additive-Free Synthesis, Remarkable Crystalline-Phase Stability, and Improved Lithium Insertion Behavior. *J. Am. Chem. Soc.* **2011**, *133*, 933−940.
(26) Duan, X.; Mei, L.; Ma, J.; Li, Q.; Wang, T.; Zheng, W. Facet-Induced Formation of Hematite Mesocrystals with Improved Lithium Storage Properties. *Chem. Commun.* **2012**, *48*, 12204−12206.
(27) Tartaj, P.; Amarilla, J. M. Multifunctional Response of Anatase Nanostructures Based on 25 nm Mesocrystal-Like Porous Assemblies. *Adv. Mater.* **2011**, *23*, 4904−4907.
(28) Uchaker, E.; Cao, G. Mesocrystals as Electrode Materials for Lithium-Ion Batteries. *Nano Today* **2014**, *9*, 499−524.
(29) Hong, Z.; Zhou, K.; Zhang, J.; Huang, Z.; Wei, M. Facile Synthesis of Rutile TiO_2 Mesocrystals with Enhanced Sodium Storage Properties. *J. Mater. Chem. A* **2015**, *3*, 17412−17416.
(30) Tartaj, P. Sub-100 nm TiO_2 Mesocrystalline Assemblies with Mesopores: Preparation, Characterization, Enzyme Immobilization and Photocatalytic Properties. *Chem. Commun.* **2011**, *47*, 256−258.
(31) Zhang, P.; Fujitsuka, M.; Majima, T. Development of Tailored TiO_2 Mesocrystals for Solar Driven Photocatalysis. *J. Energy Chem.* **2016**, *25*, 917−926.
(32) Tang, C.; Liu, L.; Li, Y.; Bian, Z. Aerosol Spray Assisted Assembly of TiO_2 Mesocrystals into Hierarchical Hollow Microspheres with Enhanced Photocatalytic Performance. *Appl. Catal., B* **2017**, *201*, 41−47.
(33) Amarilla, J. M.; Morales, E.; Sanz, J.; Sobrados, I.; Tartaj, P. Electrochemical Response in Aprotic Ionic Liquid Electrolytes of TiO_2 Anatase Anodes Based on Mesoporous Mesocrystals with Uniform Colloidal Size. *J. Power Sources* **2015**, *273*, 368−374.
(34) Hadjiivanov, K. I.; Klissurski, D. G. Surface Chemistry of Titania (Anatase) and Titania-Supported Catalysts. *Chem. Soc. Rev.* **1996**, *25*, 61.
(35) Kim, T.-W.; Kim, M.-J.; Kleitz, F.; Nair, M. M.; Guillet-Nicolas, R.; Jeong, K.-E.; Chae, H.-J.; Kim, C.-U.; Jeong, S.-Y. Tailor-Made Mesoporous Ti-SBA-15 Catalysts for Oxidative Desulfurization of Refractory Aromatic Sulfur Compounds in Transport Fuel. *ChemCatChem* **2012**, *4*, 687−697.
(36) Tanev, P. T.; Chibwe, M.; Pinnavaia, T. J. Titanium-Containing Mesoporous Molecular Sieves for Catalytic Oxidation of Aromatic Compounds. *Nature* **1994**, *368*, 321−323.
(37) Notari, B. Microporous Crystalline Titanium Silicates. *Adv. Catal.* **1996**, *41*, 253−334.
(38) Clerici, M. G. The Activity of Titanium Silicalite-1 (TS-1): Some Considerations on Its Origin. *Kinet. Catal.* **2015**, *56*, 450−455.
(39) Ratnasamy, P.; Srinivas, D.; Knözinger, H. Active Sites and Reactive Intermediates in Titanium Silicate Molecular Sieves. *Adv. Catal.* **2004**, *48*, 1−169.
(40) Mei, H.; Mei, B. W.; Yen, T. F. A New Method for Obtaining Ultra-Low Sulfur Diesel Fuel via Ultrasound Assisted Oxidative Desulfurization. *Fuel* **2003**, *82*, 405−414.
(41) Shiraishi, Y.; Hirai, T.; Komasawa, I. Oxidative Desulfurization Process for Light Oil Using Titanium Silicate Molecular Sieve Catalysts. *J. Chem. Eng. Jpn.* **2002**, *35*, 1305−1311.
(42) Kong, L.; Li, G.; Wang, X. Mild Oxidation of Thiophene over TS-1/H_2O_2. *Catal. Today* **2004**, *93*−*95*, 341−345.
(43) Jin, C.; Li, G.; Wang, X.; Wang, Y.; Zhao, L.; Sun, D. A Titanium Containing Micro/mesoporous Composite and Its Catalytic Performance in Oxidative Desulfurization. *Microporous Mesoporous Mater.* **2008**, *111*, 236−242.
(44) Yang, S.-T.; Jeong, K.-E.; Jeong, S.-Y.; Ahn, W.-S. Synthesis of Mesoporous TS-1 Using a Hybrid SiO_2−TiO_2 Xerogel for Catalytic Oxidative Desulfurization. *Mater. Res. Bull.* **2012**, *47*, 4398−4402.
(45) Kim, T.-K.; Yang, S.-T.; Park, D. R.; Song, I. K.; Jung, K.-E.; Ahn, W.-S. Ti-MWW Synthesis and Catalytic Applications in Partial Oxidation Reactions. *Top. Catal.* **2010**, *53*, 470−478.
(46) McNamara, N. D.; Neumann, G. T.; Masko, E. T.; Urban, J. A.; Hicks, J. C. Catalytic Performance and Stability of (V) MIL-47 and (Ti) MIL-125 in the Oxidative Desulfurization of Heterocyclic Aromatic Sulfur Compounds. *J. Catal.* **2013**, *305*, 217−226.
(47) Yang, H. G.; Sun, C. H.; Qiao, S. Z.; Zou, J.; Liu, G.; Smith, S. C.; Cheng, H. M.; Lu, G. Q. Anatase TiO_2 Single Crystals with a Large Percentage of Reactive Facets. *Nature* **2008**, *453*, 638−641.
(48) Selloni, A. Crystal Growth: Anatase Shows Its Reactive Side. *Nat. Mater.* **2008**, *7*, 613−615.
(49) Xu, J.; Xu, L.-F.; Li, Z.-Z.; Wang, J.-T.; Lin, Z.-S.; Liu, K.; Cao, Y.-G.; Selloni, A. Ab Initio Study of Water Adsorption and Reactivity on the (211) Surface of Anatase TiO_2. *Phys. Rev. Appl.* **2016**, *5*, 64001.
(50) Armitage, D. A.; Grant, D. M. Characterisation of Surface-Modified Nickel Titanium Alloys. *Mater. Sci. Eng., A* **2003**, *349*, 89−97.
(51) Jensen, H.; Soloviev, A.; Li, Z.; Søgaard, E. G. XPS and FTIR Investigation of the Surface Properties of Different Prepared Titania Nano-Powders. *Appl. Surf. Sci.* **2005**, *246*, 239−249.
(52) Jackman, M. J.; Thomas, A. G.; Muryn, C. Photoelectron Spectroscopy Study of Stoichiometric and Reduced Anatase TiO_2(101) Surfaces: The Effect of Subsurface Defects on Water Adsorption at Near-Ambient Pressures. *J. Phys. Chem. C* **2015**, *119*, 13682−13690.
(53) Audi, A. A.; Sherwood, P. M. A. X-Ray Photoelectron Spectroscopic Studies of Sulfates and Bisulfates Interpreted by Xα and Band Structure Calculations. *Surf. Interface Anal.* **2000**, *29*, 265−275.
(54) Patrick, C. E.; Giustino, F. Structure of a Water Monolayer on the Anatase TiO_2(101) Surface. *Phys. Rev. Appl.* **2014**, *2*, 14001.

DOI: 10.1021/acsomega.7b00307
ACS Omega 2017, 2, 2351−2359

(55) Yu, J. C.; Yu, J.; Zhao, J. Enhanced Photocatalytic Activity of Mesoporous and Ordinary TiO_2 Thin Films by Sulfuric Acid Treatment. *Appl. Catal., B* **2002**, *36*, 31−43.
(56) Tagawa, H. Thermal Decomposition Temperatures of Metal Sulfates. *Thermochim. Acta* **1984**, *80*, 23−33.
(57) Mueller, R.; Kammler, H. K.; Wegner, K.; Pratsinis, S. E. OH Surface Density of SiO_2 and TiO_2 by Thermogravimetric Analysis. *Langmuir* **2003**, *19*, 160−165.
(58) Peak, D.; Ford, R. G.; Sparks, D. L. An in Situ ATR-FTIR Investigation of Sulfate Bonding Mechanisms on Goethite. *J. Colloid Interface Sci.* **1999**, *218*, 289−299.
(59) Paul, K. W.; Borda, M. J.; Kubicki, J. D.; Sparks, D. L. Effect of Dehydration on Sulfate Coordination and Speciation at the Fe−(Hydr)oxide−Water Interface: A Molecular Orbital/Density Functional Theory and Fourier Transform Infrared Spectroscopic Investigation. *Langmuir* **2005**, *21*, 11071−11078.
(60) Yang, Q.; Xie, C.; Xu, Z.; Gao, Z.; Du, Y. Synthesis of Highly Active Sulfate-Promoted Rutile Titania Nanoparticles with a Response to Visible Light. *J. Phys. Chem. B* **2005**, *109*, 5554−5560.
(61) Raj, K. J. A.; Shanmugam, R.; Mahalakshmi, R.; Viswanath, B. XPS and IR Spectral Studies on the Structure of Phosphate and Sulphate Modified Titania—A Combined DFT and Experimental Study. *Indian J. Chem., Sect. A: Inorg., Bio-inorg., Phys., Theor. Anal. Chem.* **2010**, *49*, 9−17.
(62) Nishikiori, H.; Hayashibe, M.; Fujii, T. Visible Light-Photocatalytic Activity of Sulfate-Doped Titanium Dioxide Prepared by the Sol−Gel Method. *Catalysts* **2013**, *3*, 363−377.
(63) Marchese, L.; Gianotti, E.; Dellarocca, V.; Maschmeyer, T.; Rey, F.; Coluccia, S.; Thomas, J. M. Structure−functionality Relationships of Grafted Ti-MCM41 Silicas. Spectroscopic and Catalytic Studies. *Phys. Chem. Chem. Phys.* **1999**, *1*, 585−592.
(64) de la Peña O'Shea, V. A.; Capel-Sanchez, M.; Blanco-Brieva, G.; Campos-Martin, J. M.; Fierro, J. L. G. The Usefulness of Time-Dependent Density Functional Theory to Describe the Electronic Spectra of Ti-Containing Catalysts. *Angew. Chem., Int. Ed.* **2003**, *42*, 5851−5854.
(65) Capel-Sanchez, M. C.; Dela Peña-O'Shea, V. a.; Barrio, L.; Campos-Martin, J. M.; Fierro, J. L. G. TD-DFT Analysis of the Electronic Spectra of Ti-Containing Catalysts. *Top. Catal.* **2006**, *41*, 27−34.
(66) Ortega, Y.; Hernández, N. C.; Menéndez-Proupin, E.; Graciani, J.; Sanz, J. F. Nitrogen/gold Codoping of the TiO_2(101) Anatase Surface. A Theoretical Study Based on DFT Calculations. *Phys. Chem. Chem. Phys.* **2011**, *13*, 11340.
(67) Soria, J.; Sanz, J.; Sobrados, I.; Coronado, J. M.; Hernández-Alonso, M. D.; Fresno, F. Water−Hydroxyl Interactions on Small Anatase Nanoparticles Prepared by the Hydrothermal Route. *J. Phys. Chem. C* **2010**, *114*, 16534−16540.
(68) Sanz, J.; Soria, J.; Sobrados, I.; Yurdakal, S.; Augugliaro, V. Influence of Amorphous TiO_{2-x} on Titania Nanoparticle Growth and Anatase-to-Rutile Transformation. *J. Phys. Chem. C* **2012**, *116*, 5110−5115.
(69) Sanz, J.; Sobrados, I.; Soria, J.; Yurdakal, S.; Augugliaro, V. Anatase Nanoparticles Boundaries Resulting from Titanium Tetrachloride Hydrolysis. *Catal. Today* **2017**, *281*, 198−204.
(70) Marchese, L.; Maschmeyer, T.; Gianotti, E.; Coluccia, S.; Thomas, J. M. Probing the Titanium Sites in Ti−MCM41 by Diffuse Reflectance and Photoluminescence UV−Vis Spectroscopies. *J. Phys. Chem. B* **1997**, *101*, 8836−8838.
(71) Gao, X.; Bare, S. R.; Fierro, J. L. G.; Banares, M. A.; Wachs, I. E. Preparation and in-Situ Spectroscopic Characterization of Molecularly Dispersed Titanium Oxide on Silica. *J. Phys. Chem. B* **1998**, *102*, 5653−5666.
(72) Nitsche, D.; Hess, C. Structure of Isolated Vanadia and Titania: A Deep UV Raman, UV−Vis, and IR Spectroscopic Study. *J. Phys. Chem. C* **2016**, *120*, 1025−1037.
(73) Klissurski, D.; Hadjiivanov, K.; Kantcheva, M.; Gyurova, L. Study of Peroxide-Modified Titanium Dioxide (Anatase). *J. Chem. Soc., Faraday Trans.* **1990**, *86*, 385.
(74) Antcliff, K. L.; Murphy, D. M.; Griffiths, E.; Giamello, E. The Interaction of H_2O_2 with Exchanged Titanium Oxide Systems (TS-1, TiO_2, [Ti]-APO-5, Ti-ZSM-5). *Phys. Chem. Chem. Phys.* **2003**, *5*, 4306.
(75) Yang, C.; Zhao, K.; Cheng, Y.; Zeng, G.; Zhang, M.; Shao, J.; Lu, L. Catalytic Oxidative Desulfurization of BT and DBT from *n*-Octane Using Cyclohexanone Peroxide and Catalyst of Molybdenum Supported on 4A Molecular Sieve. *Sep. Purif. Technol.* **2016**, *163*, 153−161.
(76) Wei, S.; He, H.; Cheng, Y.; Yang, C.; Zeng, G.; Kang, L.; Qian, H.; Zhu, C. Preparation, Characterization, and Catalytic Performances of Cobalt Catalysts Supported on KIT-6 Silicas in Oxidative Desulfurization of Dibenzothiophene. *Fuel* **2017**, *200*, 11−21.
(77) González-García, O.; Cedeño-Caero, L. V-Mo Based Catalysts for Ods of Diesel Fuel. Part II. Catalytic Performance and Stability after Redox Cycles. *Catal. Today* **2010**, *150*, 237−243.
(78) Caero, L. C.; Hernández, E.; Pedraza, F.; Murrieta, F. Oxidative Desulfurization of Synthetic Diesel Using Supported Catalysts. *Catal. Today* **2005**, *107−108*, 564−569.
(79) Rivoira, L. P.; Vallés, V. A.; Ledesma, B. C.; Ponte, M. V.; Martínez, M. L.; Anunziata, O. A.; Beltramone, A. R. Sulfur Elimination by Oxidative Desulfurization with Titanium-Modified SBA-16. *Catal. Today* **2016**, *271*, 102−113.
(80) Trukhan, N. N.; Romannikov, V. N.; Shmakov, A. N.; Vanina, M. P.; Paukshtis, E. A.; Bukhtiyarov, V. I.; Kriventsov, V. V.; Danilov, I. Y.; Kholdeeva, O. A. H_2O_2-Based Selective Oxidations over Titaniumsilicates of SBA-15 Type. *Microporous Mesoporous Mater.* **2003**, *59*, 73−84.
(81) Komintarachat, C.; Trakarnpruk, W. Oxidative Desulfurization Using Polyoxometalates. *Ind. Eng. Chem. Res.* **2006**, *45*, 1853−1856.
(82) Li, L.; Zhang, J.; Shen, C.; Wang, Y.; Luo, G. Oxidative Desulfurization of Model Fuels with Pure Nano-TiO_2 as Catalyst Directly without UV Irradiation. *Fuel* **2016**, *167*, 9−16.

DOI: 10.1021/acsomega.7b00307
ACS Omega 2017, 2, 2351−2359